Energy Storage Design for Energy Harvesting Sensors

Daniel Monagle, *Graduate Student Member, IEEE*,
Thomas C. Krause, *Graduate Student Member, IEEE*,
Aaron W. Langham, *Graduate Student Member, IEEE*, and Steven B. Leeb, *Fellow, IEEE*

***Abstract*—Energy harvesting sensors scavenge energy from their surroundings to power themselves without a battery or utility-connected power supply. Sensors that avoid batteries and bespoke power wire connections offer flexibility for avoiding complications in safety and infrastructure. Energy from the sensor's environment often arrives intermittently or stochastically, complicating the sensor design process. The size of onboard energy storage becomes a critical design decision. Energy storage allows the harvesting system to accumulate energy over time that can later be consumed for sensor tasks. This article presents a modeling and design guide for sizing sensor energy storage. These guidelines balance the tension between cold-start time and steady-state endurance. Cold-start time and steady-state endurance, as a function of energy storage design parameters, are quantified and analyzed with respect to both deterministic and stochastic energy harvest profiles. Results are demonstrated using experimentally measured power consumption data from an industrial machine on a microgrid. Two practical sensor storage design examples demonstrate the design guide. Simulation results highlight the very restrictive storage unit design space over which both fast boot-up and sufficient endurance are satisfied for a notional sensor application. The negative effect of oversized storage on overall sensor ON-time over long time periods of thousands of hours is also demonstrated. These results emphasize the significant impact of storage unit start-up and maximum voltage threshold design choices and their ability to reduce a required storage capacitance by over an order of magnitude to meet the same application requirements.**

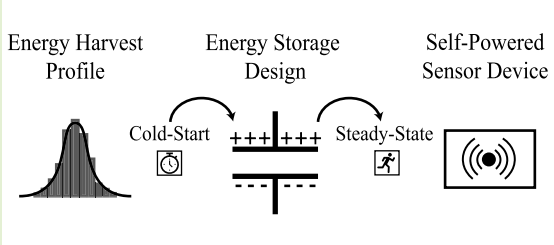

***Index Terms*—Batteryless, cold-start, energy harvesting, energy storage design, Markov chain, sensor interface electronics, stochastic.**

I. Introduction

SENSOR nodes that can "live off the land" avoid battery or bespoke power wiring requirements. The safety risks [1] of lithium-ion batteries hinder the deployment of battery-powered sensors in mission-critical settings. Energy harvesting provides an alternative. Harvesting, storing, and using energy from the sensor's ambient environment unlocks a pathway to less costly installation and reduced maintenance requirements. Furthermore, harvesting sensors can be co-deployed with batteries or other energy sources to reduce battery replacement maintenance and schedules.

Fully batteryless energy harvesting systems present unique challenges for designers. Ambient energy may arrive intermittently, and depending on the source (e.g., vibration, solar, electromagnetic radiation, etc.) may be relatively miserly. Batteryless sensors may need to perform tasks such as measurement and data transmission when little or no ambient energy is present, without relying on a battery as a stable power supply. To sustain sensor device operation over long time periods, an energy harvesting sensor must employ some energy storage. Proper design allows energy storage, like a capacitor, to hold a sufficient reservoir of harvested energy for the sensor to use as it completes tasks. Much of the self-powered sensing literature discusses sizing of the energy storage unit relative to desired sensor tasks and monitoring the stored energy to sustain operation [2], [3], [4], [5], [6], [7], [8]. Although many of these analyses recognize the intermittent nature of energy harvest, they often do not formally model ambient energy availability as a stochastic process. Additional techniques for increasing sensor lifetime and/or performance in intermittently powered energy harvesting nodes and networks include [9], [10], [11], [12]. These references augment controllers to model capacitive energy leakage [9], economically save system state just before brownouts [10], consider both sensor task energy consumption

Received 29 April 2025; revised 20 May 2025; accepted 23 May 2025. Date of publication 3 June 2025; date of current version 2 July 2025. This work was supported by the Office of Naval Research Structural Acoustics Program. The associate editor coordinating the review of this article and approving it for publication was Dr. Chung-Chih Hung. *(Corresponding author: Daniel Monagle.)*

The authors are with the Department of Electrical Engineering and Computer Science, Massachusetts Institute of Technology, Cambridge, MA 02139 USA (e-mail: monagled@mit.edu; tkrause@mit.edu; alangham@mit.edu; sbleeb@mit.edu).

Digital Object Identifier 10.1109/JSEN.2025.3573926

1558-1748 © 2025 IEEE. All rights reserved, including rights for text and data mining, and training of artificial intelligence and similar technologies. Personal use is permitted, but republication/redistribution requires IEEE permission.
See https://www.ieee.org/publications/rights/index.html for more information.
Authorized licensed use limited to: MIT. Downloaded on June 04,2026 at 16:36:13 UTC from IEEE Xplore. Restrictions apply.

and deadline requirements [11], and adjust sensor node sample frequency in response to both the signal of interest and the node's stored energy level [12]. Such examples are typically active control strategies that run in real time during sensor operation. This article, alternatively, presents tools for informing the sensor storage design process, modeling energy harvest profiles quantitatively in both deterministic (but time-varying) and stochastic cases.

Stochastic effects on energy production and harvest have been studied in some existing literature. Some works concern grid-level energy production, storage, distribution, and/or consumption [13], [14], [15], [16], [17]. For low-power sensors, existing works have analyzed the uncertainty in design parameters or excitations of vibrational energy harvesters [18], [19], [20]. Randomness in ambient wind and solar energy for predicting energy harvest in wireless sensor networks has also been studied [21]. Recent work also demonstrated Gaussian mixture model techniques to simulate the performance of a battery-powered, hybrid energy harvesting sensor system [22]. Other stochastic energy harvester works focus on optimizing task distribution or communication protocols between nodes in energy harvesting sensor networks [23], [24], [25].

Unlike some existing work that considers stochastic energy harvesting [26], our work primarily concerns the design and performance of a batteryless sensing system. Accordingly, our analysis demands modeling of the cold-start phase of a harvesting sensor, where the system boots itself up from an initial state of zero stored energy. Our modeling and design approach is illustrated with stochastic ambient energy models derived from experimental datasets of industrial equipment. Although applied to example sensors with capacitive energy storage, our approach is not specific to a particular energy harvester technology or stochastic harvest model. Rather, these example sensor designs illustrate this approach that provides statistical insights and rigor to the design process of sizing energy storage for batteryless sensing. The techniques presented in this article are broadly applicable to a variety of energy harvester technologies and sensor devices.

Previously, Munir and Dyo [27] illustrated a key design tradeoff for the storage element of a batteryless radio frequency (RF) energy harvesting sensor. Specifically, small capacitors promote fast start-up, but large capacitors are capable of servicing energy-intensive sensor tasks [27]. In response to the competing design interests and a recognition of the indeterminate nature of energy harvest, Munir and Dyo [27] introduced a Kalman filter and hybrid storage solution that actively switches between a small and large capacitor for storage, depending on the estimated available energy storage and harvest. Unlike [27], our paper emphasizes the storage unit voltage, in addition to the capacitance, as a design variable, which we demonstrate to have a significant ability to reduce capacitor sizing due to the quadratic relation between stored energy and the voltage across the capacitor. Our paper expands the storage sizing design tradeoff discussion that was presented in [27] to include rigorous mathematical formulas for sizing storage according to power harvest and sensor device power consumption profiles. While both our paper and [27] concern batteryless energy harvesters in environments where harvesting is stochastic, the methods for addressing indeterminate energy harvest are notably different. The Kalman filter strategy of [27] is especially useful for actively managing the storage unit in real-time during system operation, whereas the arrival process and Markov chain framework we present below are design tools for sizing a storage unit and estimating its start-up and long-term steady-state behavior.

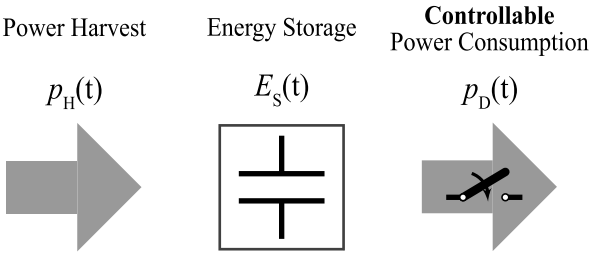

Fig. 1. Simplified power flow diagram of a batteryless energy harvesting sensor unit.

The key contribution of this article is the application of a quantitative framework to the start-up phase and steady-state operation of a batteryless sensor. With this analysis, designers can size energy harvester storage units in an informed way that accounts for variability and intermittence in energy harvesting times and magnitudes.

II. Design Goals and Problem Formulation

Fig. 1 displays a high-level power flow diagram of an idealized batteryless energy harvester sensor unit. The system contains an energy storage level $E_S(t)$ that is filled by a harvester source providing power $p_H(t)$ and drained by an attached sensor device consuming power $p_D(t)$. We have deliberately presented these as generic functions, although each energy harvester and sensor application will, of course, beget its own specific harvest and consumption profiles. For example, for a wearable sensor application, a hybrid solar-thermoelectric energy harvest profile was first experimentally recorded as subjects wore the harvester platform for several days [28]. A number of methods for predicting the hybrid harvester's energy harvest, including a modified Kalman filter, were then presented [28]. An extensive review of energy harvest prediction methods, including methods that rely purely on past harvest information, a combination of past harvest information and some environmental models, and machine learning strategies, is given by Yuan et al. [29]. As we demonstrate in Section V, a $p_H(t)$ power harvest profile can also be derived from physical models of the harvester and statistics describing the environmental conditions in the prospective harvester installation site.

Several methods exist for estimating or measuring device power consumption profiles $p_D(t)$. Simple, standard strategies are benchtop power measurements, simultaneously measuring the supply voltage of a sensor package and its current consumption for operation using digital multimeters and oscilloscopes. Recently, commercial products, such as the Joulescope, specifically tailored to power measurements and profiling of low-power embedded systems have also become available [30]. A clever approach for online sensor power

Authorized licensed use limited to: MIT. Downloaded on June 04,2026 at 16:36:13 UTC from IEEE Xplore. Restrictions apply.

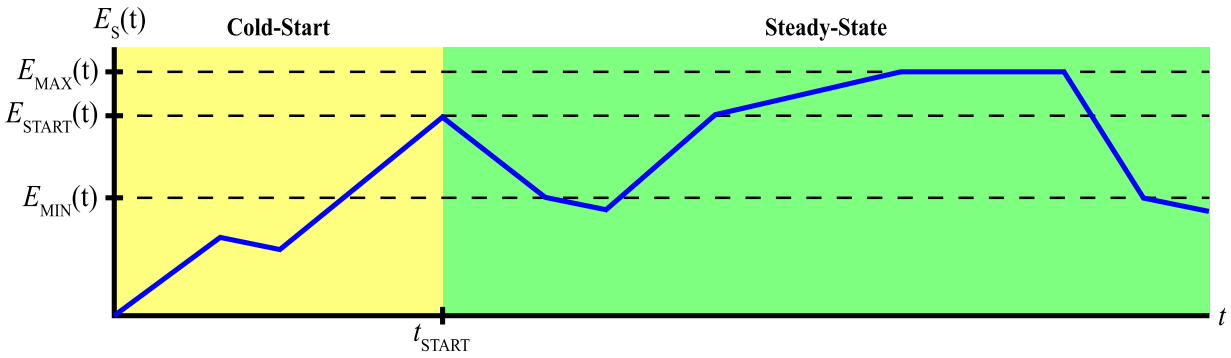

Fig. 2. Stored energy over time for the batteryless system. $E_S(t)$ varies according to (3). Self-discharge loss of the storage unit continually drains $E_S(t)$ even when the device is disabled for $E_S(t) \leq E_{MIN}$.

profiling by tracking the switching frequency of pulse frequency modulated (PFM) sensor power supplies has been proposed in existing literature [31]. Works such as [32] and [33] present mathematical models for quantifying the power consumption of low-power sensor devices at the individual component and greater system level. In sum, a $p_D(t)$ profile can be measured or estimated with existing strategies, given sensor application requirements.

Ideally, the energy storage of a batteryless sensor node is lossless, such that $E_S(t)$ remains constant when both $p_H(t)$ and $p_D(t)$ are zero. In practice, however, the energy storage will exhibit some inherent loss, due to, for example, the self-discharge characteristics of a capacitor. Generally, the lossy behavior of the storage element can be modeled by a loss profile $p_L(t)$. Fig. 2 shows key energy storage states that constrain this model. $E_S(t)$ initially charges from a completely depleted state until it reaches a critical value E_{START}, at which point an electronic control system allows the attached device to consume power. The operating regime after $E_S(t)$ has reached E_{START} and is referred to as "steady-state operation." During steady-state operation, $E_S(t)$ is ideally bounded between E_{MIN} and E_{MAX}. These limits follow from a hysteretic control scheme that disables the attached device (i.e., sets $p_D(t)$ to zero) whenever $E_S(t)$ has depleted to E_{MIN} and prevents additional energy storage above E_{MAX} by disconnecting or redirecting additional power harvest away from the storage unit. More precisely, the self-discharge $p_L(t)$ of the storage element is capable of draining $E_S(t)$ below E_{MIN} even when the sensor device is disabled. The device is re-enabled once $E_S(t)$ charges to at least E_{START} again. In its minimum and maximum bounds, $E_S(t)$ varies depending on the values of $p_H(t)$, $p_D(t)$, and $p_L(t)$.

For a capacitive energy storage unit with capacitance C, the instantaneous energy stored is

$$E_S(t) = \frac{1}{2}C[V(t)]^2 \tag{1}$$

where $V(t)$ is the instantaneous voltage across the capacitor. This work provides techniques to quantify the effect of design parameters such as C, E_{START}, and E_{MAX}, on the start-up and steady-state endurance of a batteryless sensor. A tension exists between these two problems, as a large capacitor can store significant energy for steady-state endurance, but requires a long start-up charging time. Conversely, a small capacitor charges quickly, but may not store sufficient energy to endure the sensor application's power consumption. Our goal in this article is to provide an analytical framework with which batteryless sensor designers can size energy storage.

Assuming the storage exhibits a relatively depleted energy level E_{LOW} at some time $t = t_0$, the following equation describes the cold-start time t_{START}, at which point an attached device can operate:

$$E_{START} = \frac{1}{2}CV_{START}^2 = \int_{t_0}^{t_{START}} p_H(t) - p_L(t)\,dt + E_{LOW}. \tag{2}$$

Here, E_{START} is a stored energy start-up threshold chosen by a designer. Practically, E_{START} is sized according to C and V_{START}, the voltage across the storage capacitance at time t_{START}. A conservative design, from a start-up perspective, may assume full depletion at t_0 ($E_{LOW} = 0$), but in many practical settings, a depleted storage unit will have some small but nonzero stored energy due to the inherent discharge characteristics of capacitors.

Analysis for steady-state operation focuses on the following equation:

$$\frac{dE_S(t)}{dt} = \begin{cases} -p_D(t) - p_L(t), & \forall t : E_S(t) \geq E_{MAX} \\ p_H(t) - p_L(t), & \forall t : 0 \leq E_S(t) \leq E_{MIN} \\ \Delta p(t), & \text{otherwise} \end{cases} \tag{3}$$

where

$$\Delta p(t) = p_H(t) - p_D(t) - p_L(t). \tag{4}$$

Next, we apply the above formulas to "deterministic" energy harvester cases, where energy arrives in predictable events. In Section IV, we analyze stochastic energy harvester cases, where energy harvest arrival time and magnitude are random.

III. Deterministic Energy Harvest

A deterministic power harvest profile, for example, might be described as a piecewise linear profile

$$p_H(t) = \begin{cases} 0, & 0 \leq t \leq t_1 \\ P_0, & t_1 < t \leq t_2 \\ 0, & t_2 < t \leq t_3 \\ P_1, & t_3 < t \leq t_4 \\ \cdots & \end{cases}. \tag{5}$$

Authorized licensed use limited to: MIT. Downloaded on June 04,2026 at 16:36:13 UTC from IEEE Xplore. Restrictions apply.

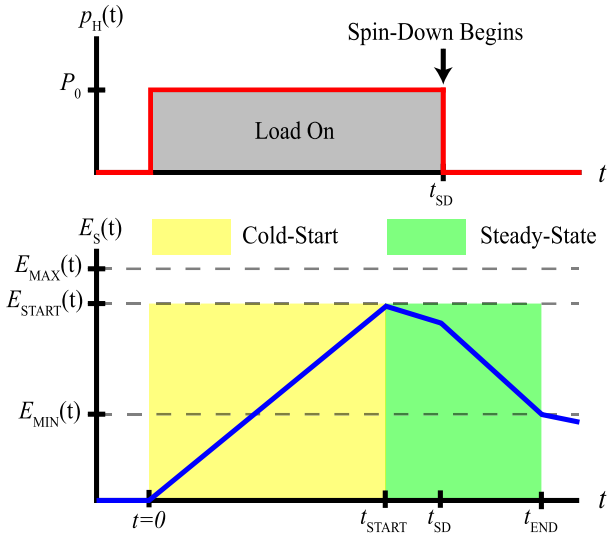

Fig. 3. Event-driven spin-down sensor cold-starts and operates to depletion per every load operating cycle. Self-discharge loss is a continuous drain on the storage for $t > 0$, and its effect continues to slowly drain the stored energy even after the device is disabled at t_{END}.

Another harvest example is a completely constant profile

$$p_H(t) = P_0. \tag{6}$$

More complex, but well-characterized functions, like sinusoids or pulsatile waveforms, may also represent deterministic energy harvest for other harvester technologies. Given $p_H(t)$, our design goal is to size an energy storage unit that meets both a minimum start-up time specification and a minimum sensor ON-time duration over a steady-state time interval of interest.

While sensor nodes have a variety of use profiles, one can consider the broad class of "event-driven" sensors. An event-driven sensor must detect and record information in response to the occurrence of a specific "event" in its environment. Example applications of event-driven sensors are found in insect and plant monitoring [34], camera-based object detection [35], and spin-down monitoring of industrial machines [36], [37]. Many event-driven sensors are prime candidates for batteryless sensing. This guide allows informed energy storage design for such sensors.

Consider, for example, the design of a spin-down sensor for a rotating electromechanical machine [36], [37]. A batteryless magnetic energy harvester-equipped sensor, for example, could power itself by harvesting energy from the magnetic fields present around the machine's wires as this load draws electrical current. As shown in Fig. 3, the event-driven sensor cold-starts, performs its tasks, and depletes its storage, in response to a single operating cycle event of the electromechanical load it senses. Assuming fixed minimum and maximum voltage bounds, V_{MIN} and V_{MAX}, on the capacitor, the challenge is finding a C and V_{START} combination that allows the unit to complete start-up before t_{SD}, while also storing enough energy to perform the sensing application once the device is enabled. Throughout the analysis below, we assume a constant loss characteristic $p_L(t) = P_L$ for simplicity.

A. Cold-Start Analysis

With reference to (2), let $t_0 = 0$ and assume $E_{LOW} = E_S(t_0) = 0$. This assumption of total depletion at time t_0 in the following analysis provides a conservative design, which demands the storage must be capable of charging from a state of full depletion during the harvest event. Under these assumptions, an integration of (2) yields t_{START} for a given E_{START}. For a constant power harvest profile, we have

$$t_{START} = \frac{E_{START}}{P_0 - P_L} = \frac{C V_{START}^2}{2(P_0 - P_L)}. \tag{7}$$

The success criterion for cold-start time is

$$t_{START} \leq t_{SD} - \epsilon \tag{8}$$

where ϵ represents any nonnegligible initialization time for the sensor device that occurs between when it is first enabled at t_{START} and when it can begin performing its core task(s). If the cold-start success criterion is not met, then the system has not booted up fast enough to sense the event of interest.

B. Steady-State Endurance

After start-up, the sensor begins the operation of its task(s). For simple illustration, we now assume a constant power harvest profile $p_H(t) = P_0$, a sensor device power consumption $p_D(t) = P_D > P_0$ when enabled, and a device operation time specification Δt_D that is the necessary runtime for the device to complete its task. An event-driven sensor operates for a time duration

$$\Delta t_{ON} = \Delta t_{ON,A} + \Delta t_{ON,B} \tag{9}$$

where $\Delta t_{ON,A}$ and $\Delta t_{ON,B}$ represent the subdurations of Δt_{ON} over which $p_H(t) \neq 0$ and $p_H(t) = 0$, respectively. For the constant power harvest profile $p_H(t) = P_0$, we have

$$\Delta t_{ON,A} = \frac{E_S(t_{SD}) - E_{START}}{P_0 - P_D - P_L} \tag{10}$$

and

$$\Delta t_{ON,B} = \frac{E_{MIN} - E_S(t_{SD})}{-P_D - P_L} \tag{11}$$

where $E_S(t_{SD})$ is the stored energy at the spin-down time. If $\Delta p(t)$ is sufficiently negative, the device will black out before time t_{SD} due to depleted storage, and thus $\Delta t_{ON,B} = 0$. This yields a total runtime

$$\Delta t_{ON} = \frac{E_{MIN} - E_{START}}{P_0 - P_D - P_L}. \tag{12}$$

If the event-driven application requires sensing for $t > t_{SD}$, then this design has failed. Otherwise, the design has succeeded as long as $\Delta t_{ON} \geq \Delta t_D$.

If $\Delta p(t)$ is not sufficiently negative to deplete the storage prior to t_{SD}, then $E_S(t_{SD}) > E_{MIN}$ and $\Delta t_{ON,B} > 0$. With reference to the spin-down sensor of Fig. 3

$$\Delta t_{ON,A} = t_{SD} - t_{START} \tag{13}$$

and

$$\Delta t_{ON,B} = t_{END} - t_{SD}. \tag{14}$$

Authorized licensed use limited to: MIT. Downloaded on June 04,2026 at 16:36:13 UTC from IEEE Xplore. Restrictions apply.

The total ON-time of the load and t_{SD} can be determined from measured electromechanical load profile statistics, as will be demonstrated in the case study of Section V. Since each E_{START} in the design space yields a known t_{START} according to (7), $\Delta t_{ON,A}$ can be calculated using (13). Combining (10) and (13) yields a solution for $E_S(t_{SD})$, from which $\Delta t_{ON,B}$ can be calculated to obtain the total runtime according to (9).

The steady-state success criterion for an event-driven sensor is generally described as follows:

$$\Delta t_{ON} \geq \Delta t_D. \tag{15}$$

If this success criterion is not met, then the device has blacked out before completing its application due to depleted energy storage. Further constraints on this success criterion, such as the necessity for sensing during $t > t_{SD}$, can be added for each event-driven sensor's target application. It is relevant to note that the device runtime Δt_D and power consumption P_D could also exhibit some variability. While the sensor designer can assert a great degree of control on the sensor power consumption profile $p_D(t)$ by implementing a deterministic task schedule or application, the designer should also be mindful of tasks that are especially vulnerable to consumption profile variability. A wireless data transmission task, for example, from the sensor node to a central beacon could be subject to network latency that manipulates the "ideal" device power consumption profile. In such cases, a designer should use a device consumption profiling technique, like those described in Section II, to characterize $p_D(t)$ variability. With a better understanding of the sensor task uncertainty, one can adjust Δt_D or P_D accordingly to reflect worst case profile conditions and produce a conservative storage design.

This section analyzed cold-start time and steady-state endurance under known power harvest conditions. For event-driven sensors, even if the occurrence of nonzero $p_H(t)$ harvest events are infrequent or stochastic, the duration and magnitude of nonzero power harvest may be well known. The sensor can be designed to boot up, operate, and deplete on a "per-event" basis according to the equations presented above.

Alternatively, one can consider a "time-distributed" sensing application. In time-distributed sensing, tasks are not intended to be performed in response to specific environmental triggers. Instead, the sensor should exhibit a high ON-time over long timescales, between nonzero power harvest events. A stochastic framework can account for randomness in both arrival time and magnitude of energy harvest over long time periods.

IV. Stochastic Energy Harvest

In many energy harvesting application spaces, the ambient energy availability is nondeterministic. For example, sunlight, wind, and industrial load patterns are often characterized by probability distributions [17], [26], [38]. These random inputs make start-up time and steady-state behavior probabilistic. Probabilistic modeling and data analysis provide statistical measures of start-up time and steady-state operation to aid the storage design of a self-powered sensor. This probabilistic analysis is especially useful for time-distributed sensing. In contrast to event-driven sensing, time-distributed sensing does not demand sensing in response to a specific environmental trigger. Instead, the design goal is to maintain a large fraction of sensor ON-time even when power is not being actively harvested. This section models energy harvest opportunities that occur randomly as arrival processes. Start-up time is quantified from the interarrival times and magnitudes of energy harvest events. Steady-state endurance is estimated using a Markov chain framework, where the stored energy is described by a Markov state space. The state space is traversed according to stochastic energy harvest events, deterministic device consumption, and storage self-discharge.

A. Cold-Start Analysis: Arrival Process

Arrival processes model random discrete events on a system of interest. Considering random energy harvest opportunities as an arrival process allows for a quantification of cold-start time, even when power harvest is nondeterministic. Armed with a probability distribution of harvest opportunities, a designer can use the following tools to predict the start-up time of a batteryless sensor.

For any arrival process, the time S_n of the nth arrival into the system is the sum of the interarrival times over $[1, n]$. That is,

$$S_n = \sum_{i=1}^{n} X_i \tag{16}$$

where X_i is the ith interarrival time of the stochastic harvest profile. During start-up, the device is disabled, and a fixed amount of energy E_{in} is accumulated in the storage after each harvest event. The distribution of S_n describes the start-up behavior of this energy harvesting sensor. The value of n for which $E_S(S_n)$ is greater than E_{START} corresponds to the number of energy harvest events required to cold-start, for lossless storage. Given a probability distribution of X_i and this number of events, (16) yields the distribution of the time required for all of these events to arrive. From this distribution, a designer can derive statistics such as the expected cold-start time.

One can consider, for example, a batteryless magnetic energy harvester installed on the electrical cabling of an industrial heater or motor with the intent of measuring temperature in the nearby environment throughout the day. This first design question concerns how long it will take, or in other words, how many energy harvest arrivals must occur, for this sensor to boot up and begin sensing. If the energy harvesting interarrival times are well modeled as exponential random variables, the process is Poisson and each X_i has a cumulative distribution function (cdf)

$$F_{X_i}(x) = 1 - e^{-\lambda x} \tag{17}$$

where X_i is the random variable and λ is the rate parameter that characterizes the Poisson process. The sum of N independent exponential random variables with rate parameter λ is Gamma-distributed. Thus, the nth arrival time is distributed as a Gamma random variable with $\alpha = n$ and $\beta = \lambda$, that is, $S_n \sim \Gamma(\alpha = n, \beta = \lambda)$ [39].

Authorized licensed use limited to: MIT. Downloaded on June 04,2026 at 16:36:13 UTC from IEEE Xplore. Restrictions apply.

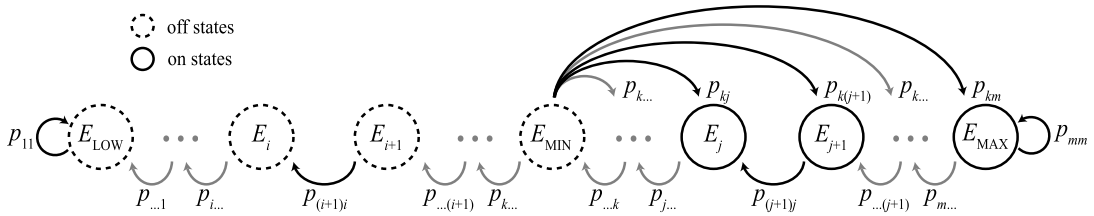

Fig. 4. Energy harvester state space. For clarity, the complete transition path arrows to higher energy states are only shown for the E_{MIN} state. The E_{MIN} state is shown corresponding to the kth element of the transition matrix.

The number of arrivals to reach a desired energy level E_{START} is

$$N_{\text{START}} = \left\lceil \frac{E_{\text{START}}}{E_{\text{in}}} \right\rceil. \tag{18}$$

The distribution of the "N_{START}th" arrival time ($S_{N_{\text{START}}}$) provides insight into the required start-up time of a harvester connected to a load with a specific statistical turn-on profile. The impact of lossy storage may be significant if start-up time or loss terms are large. A check on the estimated start-up time versus storage loss models can reveal whether the start-up time estimate is reasonable or if additional modeling or correction factors are necessary. For example, if the sensor would nominally start-up within a few hours and the storage losses would require many days to drain the storage unit, the lossless assumptions should provide reasonable estimates.

This arrival process framework also supports analysis when both the magnitude and times of harvested energy are random. For example, for the same arrival process but with independent and identically distributed (IID) energy harvest magnitudes, the stored energy becomes a compound Poisson random variable

$$E_{\text{S}}(t) = \sum_{i=1}^{N(t)} E_{\text{in},i} \tag{19}$$

where $N(t)$ is the Poisson-distributed integer-valued number of arrivals at some time t and $E_{\text{in},1}, E_{\text{in},2}, \ldots, E_{\text{in},N(t)}$ are IID random variables that describe the energy harvest for the ith harvest event. A characterization through moments (expected value and variance) and probability inequalities provide informative expressions on expected cold-start time.

B. Steady-State Endurance: Discrete-Time Markov Chain

Our steady-state design goal in time-distributed sensing applications is to ensure high device ON-time between energy harvest opportunities. To quantify the steady-state endurance of the energy harvesting sensor in stochastic cases, a Markov chain approach is proposed. Stored energy levels are discretized into the states of a Markov chain. The stochastic harvesting, as well as the self-discharge of the storage and the controlled device power consumption, are captured as probabilistic transitions between the stored energy states. Fig. 4 shows a diagram of the Markov chain state space for the energy harvesting sensor. At any integer multiple of a time step Δt, the model assumes E_{S} is equal to some level in this state space. The stored energy traverses this state space due to energy harvest, energy consumption, and self-discharge. The state space is constrained within E_{LOW} and E_{MAX} bounds as described above. The Markov analysis presented here accommodates lossless or lossy energy storage. Similar to Section III, the analysis in this section uses a constant storage loss term $p_{\text{L}}(t) = P_L$.

In general terms, the Markov property defines Markov models and states as follows:

$$\begin{aligned} &\mathbb{P}\{X_{n+1} = j | X_n = i, X_{n-1} = k, \ldots, X_0 = l\} \\ &\quad = \mathbb{P}\{X_{n+1} = j | X_n = i\}. \end{aligned} \tag{20}$$

That is, the random variable X_{n+1} (the next state) depends on the past random variables only through the most recent random variable X_n (the current state). The probability of jumping from state $i \in \mathcal{S}$ to some other state $j \in \mathcal{S}$ at the next time index is a transition probability, denoted as p_{ij}. The transition probability matrix P fully characterizes a discrete-time finite Markov chain

$$P = \begin{bmatrix} p_{11} & p_{12} & \cdots & p_{1m} \\ p_{21} & \ddots & & \\ \vdots & & & \\ p_{m1} & & & p_{mm} \end{bmatrix}. \tag{21}$$

This Markov chain framework provides an extremely valuable design insight. Building P, calculating P^{∞}, and evaluating the resulting matrix reveals the fraction of time spent in each stored energy state over the long run. Thus, faced with stochastic harvesting, a designer can confidently estimate the amount of time the device operates according to the amount of time spent in energy states greater than E_{START}. The construction of the state space and probability matrix are essential steps for this powerful design tool. In a time-distributed sensing application, the device has two distinct modes of operation: "on" and "off." If $E_{\text{S}}(t) > E_{\text{MIN}}$, the device is on and sensing. If $E_{\text{S}}(t) \leq E_{\text{MIN}}$, the device is off and not sensing. The two modes partition the Markov chain state space, such that each state belongs to one of the two modes. In the off region of the state space, adjacent levels of state space are spaced by $E_{\text{STEP,OFF}} = (\Delta t)P_L$. In the on region of the state space, adjacent state space levels are spaced by $E_{\text{STEP,ON}} = (\Delta t)(P_D + P_L)$. These are the amounts of energy dissipated over Δt in each operating mode. The number of levels in the state space is either set explicitly and the corresponding Δt is automatically calculated from above, or the Δt is set and the number of levels calculated.

The transition probability matrix entries require the probability that a harvest event arrives over the time interval of interest and the probability that the storage gains certain amounts of energy as a result. For example, in a Poisson

Authorized licensed use limited to: MIT. Downloaded on June 04,2026 at 16:36:13 UTC from IEEE Xplore. Restrictions apply.

arrival process, the probability that an arrival occurs within the timestep Δt is

$$\mathbb{P}\{\text{Arrival in } \Delta t\} = \lambda(\Delta t)e^{-\lambda(\Delta t)}. \tag{22}$$

For a small Δt, the probability of two or more arrivals is small and approximated as zero. Therefore, the probability of no arrival in Δt is one minus the above single-arrival probability. The harvester transitions to the lower energy state with a probability of no harvest arrival. Otherwise, the harvester transitions to a higher energy state with the probability of an arrival in Δt and the probability that an appropriate net energy has been accumulated. For example, the transition probability to jump three energy levels in the state space is

$$\mathbb{P}\left\{(\text{Arrival in } \Delta t) \cap \left(\left\lfloor \frac{E_{\text{NET}}}{E_{\text{STEP}}} \right\rfloor = 3\right)\right\} \tag{23}$$

where $E_{\text{NET}} = E_H - (E_D + E_L)$, the difference of harvested energy and the total drain on the storage (the sum of device-consumed energy plus storage self-discharge energy) for the arrival event. Arrival time and energy harvest are assumed independent, and this probability simplifies to multiplication of the probabilities of the individual events. The details of a specific power harvest profile dictate the distribution of E_{NET}.

The above analysis demands modeling approximations to ensure that the Markov property (i.e., that the next state depends only on the present state) is not violated. First, a hysteretic controller, which is inherently not memoryless of state, violates the Markov property. Thus, as mentioned before, this analysis uses $E_{\text{START}} = E_{\text{MIN}} + E_{\text{STEP,ON}}$. In other words, the sensor device is enabled whenever stored energy is greater than E_{MIN}, eschewing hysteresis modeling. Next, in general, the power harvest and dynamics of the stored energy depend on the duration of energy harvest events. This temporal dependency, a timekeeping of nonzero power harvest durations, violates the Markov property. Alternatively, if nonzero energy harvest ($p_{\text{H}}(t) > 0$) ON-times are compressed into a single time instant, the Markov property holds. This adaptation confines the Markov chain analysis to times when power harvest is zero and is referred to in this article as "compressed time." This is suitable for self-powered sensor cases in which the instantaneous power harvest is much greater than the device's power requirement. In other words, device operation is guaranteed when energy harvest is nonzero. In the compressed time framework, there are only two possibilities at each time step: either a nonzero harvest event occurs or it does not. If a nonzero harvest occurs, the stored energy transitions to the state corresponding with the change in stored energy during that harvest event, and the model "fast forwards" to the time instant directly after the power harvest has returned to zero. Fig. 5 illustrates the compressed time paradigm for a single nonzero harvest event. The leftmost figures show $p_{\text{H}}(t)$ and $E_{\text{S}}(t)$ over a period where harvesting begins at time t_0. The harvester gains enough energy that, when the harvesting event ends, $E_{\text{S}}(t)$ is at a higher energy level than when the event began. The rightmost figures show the compressed-time analog to the leftmost plots. In compressed time, the harvested power is an impulse, or delta function, and the energy accumulation E_{NET} happens at one instant as a step change. When power harvest is zero, compressed time is the same as "real" time, and the harvester depletes some energy and transitions down one energy state as a device consumes power and as the storage element self-discharges.

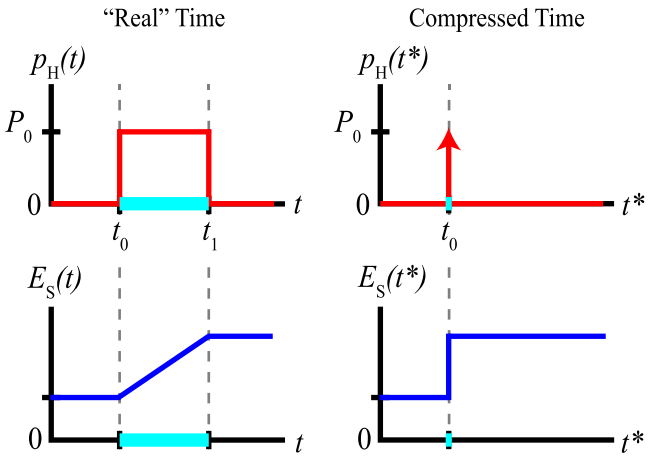

Fig. 5. Compressed time example of a harvest event.

In summary, this framework establishes a recurrent Markov chain of discrete stored energy states that are traversed according to device power consumption, lossy storage, and stochastic energy harvest arrivals. A transition matrix P can be constructed based on the probabilities of harvest opportunities, and estimating P^{∞} using numerical tools reveals the long-term steady-state convergence to each stored energy state, and thus the enduring sensor device ON-time. Section V-E demonstrates this process to design the storage stage of a self-powered temperature sensor.

V. Shipboard Load Case Study With Sensor Design Examples

Although the energy storage framework presented above is generally applicable to a variety of harvester sources and sensor devices, this section presents a representative example design focused on magnetic energy harvesting. This section presents measured field data of a candidate load for magnetic energy harvesting on a marine microgrid. This data informs two distinct harvester storage design cases: one targeting an event-driven vibration sensor and the other a time-distributed temperature sensor. To gather the data, a nonintrusive load monitor (NILM) was installed on an engine room panel on a United States Coast Guard (USCG) patrol boat. This vessel uses a three-phase 440-V (line-to-line, rms) power grid for its electrical loads. The NILM measures the line-to-line voltage waveforms and the line current waveforms at an aggregate metering point upstream of the ship's electrical loads. Real and reactive power spectral envelopes are extracted from the current and voltage data. The resulting stream contains a record of every electrical load actuation.

Postprocessing techniques disaggregated individual load power signatures and actuation times over an approximately two-month time period. Further processing generated load statistics relevant to magnetic energy harvesting from these signatures and schedules. Section V-A discusses the candidate load identified for energy harvesting. Section V-B maps the

Authorized licensed use limited to: MIT. Downloaded on June 04,2026 at 16:36:13 UTC from IEEE Xplore. Restrictions apply.

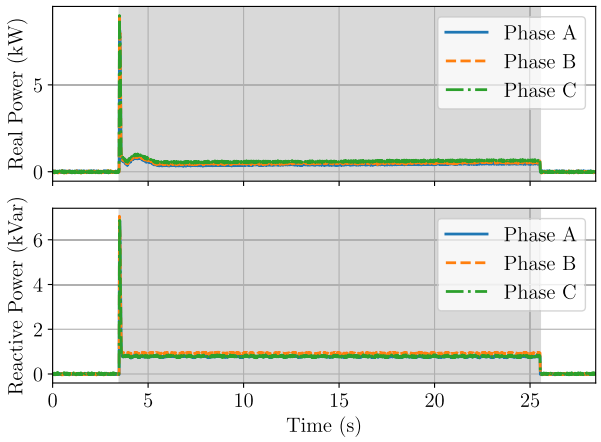

Fig. 6. Real and reactive per-phase power for one run of the vacuum pump described in Section V-A. The pump is on during the shaded interval.

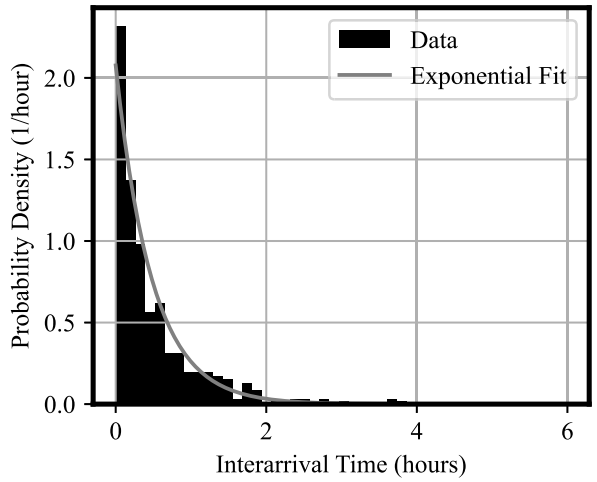

Fig. 7. Histogram of interarrival times for each sewage vacuum pump actuation.

load statistics to a power harvest profile $p_{\mathrm{H}}(t)$ for use in sizing storage. Sections V-C–V-E present harvester design parameters and simulation results for the designed energy storage units in multiple sensor applications.

A. Vacuum Pump

USCG cutter Sturgeon, an 87' patrol boat, uses a vacuum-powered sewage system. To create the vacuum, a vacuum pump is controlled to maintain a pressure setpoint. This pump is driven by a three-phase, grid-connected induction machine. Fig. 6 shows the disaggregated real and reactive per-phase power of a typical vacuum pump run. An event detection filter and a clustering algorithm identified each actuation of the pump during underway periods, that is, when the ship was out at sea. Taking the difference between each successive pump turn-on event's timestamp yielded the interarrival times for the pump. Fig. 7 shows a histogram of these interarrival times. The empirical values exhibit a good fit with an exponential distribution fit with rate parameter $\lambda = 2.08$ actuations per hour.

For each actuation, the per-phase steady-state apparent power was extracted. Dividing this by the line-to-neutral rms voltage yielded the per-phase rms current consumed by this machine for each actuation. A histogram of these rms current values for each actuation is shown in Fig. 8(a). Every actuation had an associated duration or run time. Subtraction of consecutive on-event and off-events yields a sample of durations. Fig. 8(b) shows a histogram of the run times. Multiplication of the steady-state current by the actuation run time yields the total "amp-seconds" of the load actuation. This quantity is proportional to the total energy harvested by a connected magnetic energy harvester. Fig. 8(c) shows the histogram of amp-seconds for each pump run. Table I summarizes the statistics of the vacuum pump with means and standard deviations.

TABLE I
VACUUM PUMP STATISTICS WHILE UNDERWAY

	Current (A_{rms})	Duration (s)	Amp-Seconds (A_{rms} s)
Mean (μ)	3.23	30.40	97.76
Std. Dev. (σ)	0.15	6.73	20.63

B. Energy Harvesting Profile

A power harvest profile $p_{\mathrm{H}}(t)$ is necessary to inform and verify our energy harvester sensor design examples. Here, we focus on a magnetic energy harvester, but an analogous approach could be applied to different harvester technologies (piezoelectric, solar, thermoelectric, etc.) once statistics of the appropriate available ambient energy (vibration patterns, solar patterns, and temperature differentials) for each transducer technology are obtained. Magnetic energy harvesters scavenge energy from the magnetic fields surrounding conductors according to Faraday's Law. These harvesters are often configured as current transformers and consist of a magnetic core clamped around the conductor from which energy is harvested. Our previous work has recorded the average maximum power harvest densities of several state-of-the-art examples in existing literature [40]. These power harvest densities range from 0.2 to 5.3 mW/(cm^3 · A_{rms}), where the power density is normalized by the cubic volume of the harvester core material (in cm^3) and the rms current flowing through the conductor from which the harvester scavenges energy (A_{rms}) [40]. A nominal power harvest density of 2.0 mW/(cm^3 A_{rms}) is used in the design examples below, and we assume this power harvest density holds whenever the load is on. Otherwise, the power harvest is zero. The following examples assume a harvester installed on a single conductor phase of the vacuum pump, whose load statistics provide practical A_{rms} values for use in determining a specific power harvest profile in the sensor deployment environment. Furthermore, we assume a magnetic core volume of 5.45 cm^3, which is the core volume of our recently demonstrated batteryless sensor [3].

C. Harvester and Electronic Parameters

Sections V-D and V-E present energy harvesting sensor design examples. The goal of Sections V-D and V-E is not to provide exhaustive results for all sensor applications. Rather, we aim to present two complementary, practical sensor design examples that illustrate the usefulness of our general start-up

Authorized licensed use limited to: MIT. Downloaded on June 04,2026 at 16:36:13 UTC from IEEE Xplore. Restrictions apply.

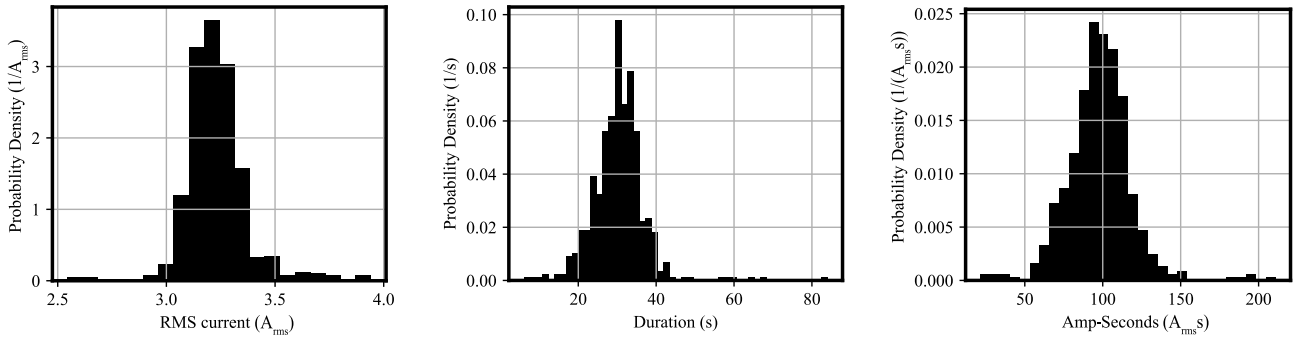

Fig. 8. Load histograms. (a) Steady-state per-phase rms current. (b) Run duration. (c) Pairwise multiplication of rms current and duration.

and steady-state analysis framework presented above. The first design example is an event-driven sensor design, where E_{START} is the key design variable of interest. The second design example is a time-distributed sensor design, where E_{MAX} is the key design variable, and the device is enabled whenever E_{S} is greater than E_{MIN}. We assume for both examples that each batteryless sensor package is powered by a current transformer magnetic energy harvester described in Section V-B.

The design is further constrained by restricting storage capacitor values and voltages within practical ranges of [10^{-6}, 1 F] and [0.6, 10 V], respectively. The wide capacitor value range, practically, spans a variety of capacitor technologies, from ceramic or metal film up to supercapacitors. For both the following design examples, we assume a conservative constant capacitor self-discharge current of 5 μA, which is on the order of the 1.45 μA self-discharge current of a typical, commercially available 1-F supercapacitor [41]. We further assume a conservative capacitor voltage level of 10 V, the largest voltage in our design space, for our loss characteristic, such that

$$p_L(t) = P_L = 5\ \mu\text{A} \cdot 10\ \text{V} = 50\ \mu\text{W} \tag{24}$$

in both the event-driven and time-distributed designs.

D. Event-Driven Sensor Design

The event-driven sensor design is motivated by electromechanical spin-down sensor applications, like those described in [36] and [37]. Sensing vibration and back EMF data during a motor spin-down can reveal critical insights into machine health that may be masked during the machine's steady-state rotational operation. Here, there is little to no benefit to operating the sensor device between vacuum pump operations. Instead, the sensor must successfully cold-start within the motor's electrical ON-time and maintain its own sensor ON-time long time to capture motor spin-down information before depleting the storage unit. This presents a prime example of competing design interests. A small energy storage will satisfy quick start-up but fail to maintain device operation for a sufficient period of time. A large storage will maintain sufficient device operation, but will not cold-start fast enough to capture the desired spin-down event to sense.

According to the vacuum pump statistics presented above, 2.6 A_{rms} was the lowest observed current draw of the induction machine. Thus, a constant power harvest magnitude

$$p_{\text{H}}(t) = P_0 = 2.6\ \text{A}_{\text{rms}} \cdot \frac{2.0\ \text{mW}}{\text{cm}^3\text{A}_{\text{rms}}} \cdot 5.45\ \text{cm}^3 = 28.34\ \text{mW} \tag{25}$$

was assumed. A constant device power consumption $p_{\text{D}}(t) = P_D = 50$ mW was also assumed, representing a relatively power-hungry sensor package. The start-up time specification was chosen as 90% of the load "on" duration. The device runtime specification Δt_D was chosen as the sum of the remaining 10% of load ON-time and five additional seconds for spin-down sensing. An additional steady-state success criterion for this spin-down design example was that $\Delta t_{\text{ON,B}}$, the device runtime after t_{SD}, must be greater than or equal to the 5 s allotted for spin-down sensing. Consistent with a conservative design, the storage is assumed completely depleted at $t = 0$.

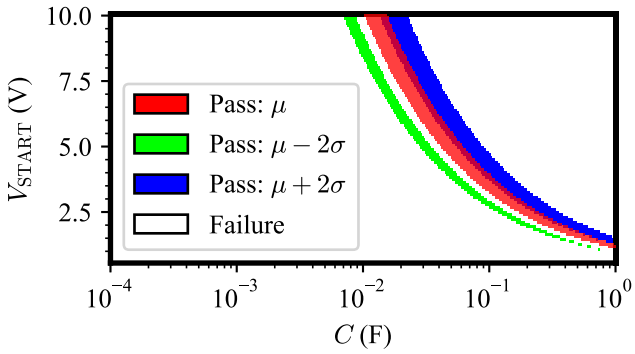

Fig. 9. 2-D mapping of the V_{START} and C design space for three event-driven sensor designs.

Fig. 9 plots the C and V_{START} combinations for which both the cold-start and steady-state specifications are met. Successful, passing designs are shown for example that assume the load ON-time is its mean value (μ) recorded in Table I, as well as the mean ON-time plus or minus two standard deviations ($\pm 2\sigma$). These deviation choices are arbitrary and purely illustrative, corresponding to strictly positive on-durations of different lengths to demonstrate each case's successful design space. Although Fig. 9 shows the effect of deviations in load ON-time, similar design maps can be produced concerning variation in other design parameters, such as power harvest magnitude, start-up time requirements, or steady-state

Authorized licensed use limited to: MIT. Downloaded on June 04,2026 at 16:36:13 UTC from IEEE Xplore. Restrictions apply.

endurance requirements. As discussed in Section III-B, device consumption variability could be a notable concern in certain applications. A design map that highlights successes and failures over multiple Δt_D and P_D variations could prove especially useful for such designs. This example demonstrates the extremely restricted E_{START} design space over which the event-driven spin-down sensor meets its application requirements in a realistic deployment scenario.

E. Time-Distributed Sensor Design

This time-distributed sensor design is broadly motivated by environmental and asset monitoring applications. Such applications involve periodic measurements of temperature, air quality, humidity, and so on to track the health of a machine or working environment. This section uses the analysis and equations in Section IV with the statistical load profile above to design the storage stage of a magnetic energy harvester intended to sense temperature. A temperature sensor serves as a concrete example, but the analysis and design objective can apply to other sensor types. The design goal is to maximize sensor ON-time and minimize the storage capacitor for size, cost, and start-up reasons. In contrast to the event-driven case, this design assumes $V_{\text{START}} = V_{\text{MIN}}$ and explores E_{MAX} as a design variable according to combinations of V_{MAX} and C.

1) Start-Up: Multiplication of the amp-second histogram values with the harvester power density and core volume yields the estimated energy harvests for each electromechanical load turn-on event. The average harvested energy per harvest event exceeded 1 J. Even with the largest capacitor value included in our design space, $C = 1$ F, the start-up threshold $E_{\text{MIN}} = E_{\text{START}} = (1/2)CV_{\text{MIN}}^2 = 0.18$ J. In this design example, due to large harvests and low $V_{\text{MIN}} = 0.6$ V, the harvester cold-starts within the first load turn-on event for all capacitance values in the design space $C = [10^{-6}, 1\text{ F}]$. Therefore, regardless of capacitance value, the start-up time is the first harvest arrival time, which is an exponentially distributed random variable. The additional modeling of Section IV-A would apply if the E_{MIN} threshold was higher or the harvest values were lower such that it took multiple load turn-on events to accumulate charge and start-up the device. This occurs with higher V_{MIN}, larger capacitor values, lower harvester power density, and lower load current consumption.

2) Steady State: In a steady state, the harvest values minus the energy drain from the storage element (duration times the sum of device power consumption and storage self-discharge) yield samples of the net energy harvested, E_{NET}, for each harvest event. Fig. 10 shows a histogram of the net energy harvested for a device power consumption $p_{\text{D}}(t) = 1$ mW and self-discharge $p_{\text{L}}(t) = 50\ \mu$W. A Gaussian fit reasonably models the data, with an average net harvest of 1.034 J and a standard deviation of 0.22 J. This Gaussian distribution and the rate parameter λ feed probability calculations which comprise the Markov chain transition probability matrix. The simulation approximates P^{∞} and uses the first row of the result to estimate the steady-state probabilities of the Markov chain. The full simulation parameters were as follows.

1) $p_{\text{D}}(t) = 1$ mW.
2) $p_{\text{L}}(t) = 50\ \mu$W.

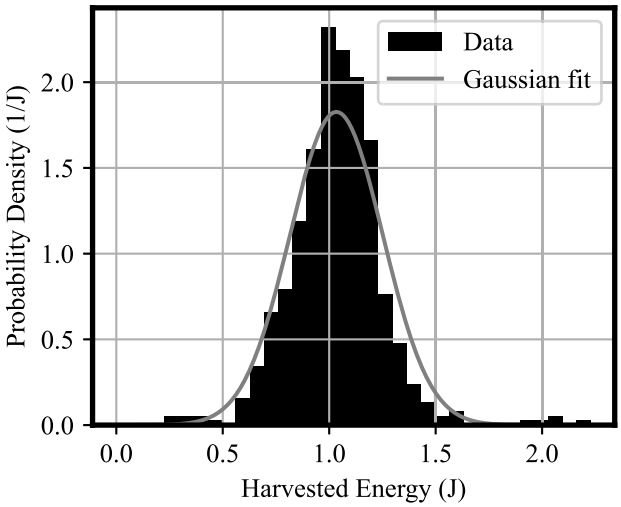

Fig. 10. Histogram of net harvested energy per energy harvest arrival.

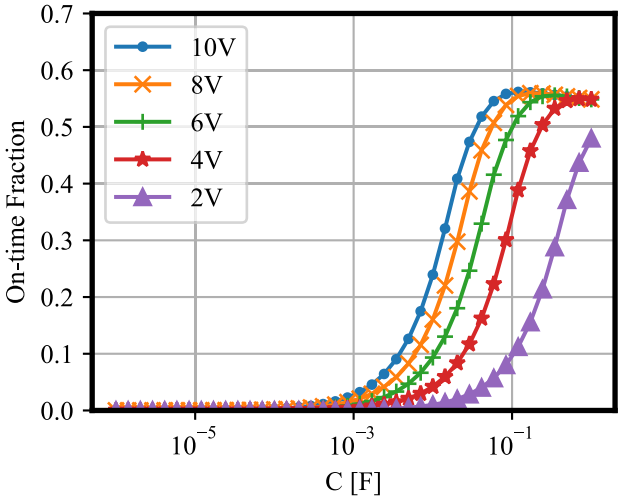

Fig. 11. Markov analysis demonstrates sensor ON-time for a variety of C and V_{MAX} design possibilities.

3) $V_{\text{MIN}} = V_{\text{START}} = 0.6$ V.
4) $V_{\text{MAX}} = [2, 10\text{ V}]$.
5) E_{NET} Distribution: $\mathcal{N}(\mu = 1.034\text{ J}, \sigma = 0.22\text{ J})$.
6) Load Rate Parameter: $\lambda = 2.08$ arrivals per hour.
7) $\Delta t = 5$ s.

Fig. 11 shows the result of five Markov chain analyses and plots the fraction of compressed time that the sensor is operational versus the storage capacitor size. Simulations across five values of V_{MAX} demonstrate how the maximum voltage rating affects steady-state sensor endurance. For this set of simulations, the $V_{\text{MAX}} = 10$ V curve maximizes ON-time for any given capacitor value and provides the largest ON-time of about 56.2% at a capacitor value of 0.12 F. Beyond this capacitance value, the $V_{\text{MAX}} = 10$ V curve decreases because the probability that the extra storage capacity is used becomes so small given the arrival rate of the energy harvest events, while the increased E_{MIN} threshold limits device operation. Interestingly, because all the V_{MAX} designs share the same V_{MIN}, the curves converge at large capacitance values once each of their E_{MAX} values is sufficiently large for this energy harvesting environment. This Markov analysis reveals some key design insights. First, it demonstrates that, for a given

Authorized licensed use limited to: MIT. Downloaded on June 04,2026 at 16:36:13 UTC from IEEE Xplore. Restrictions apply.

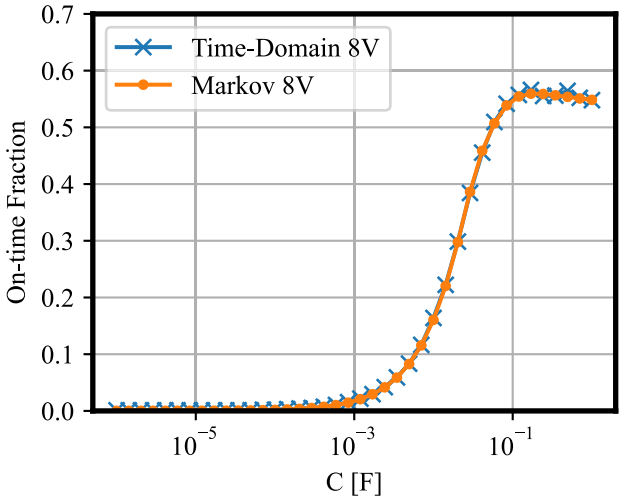

Fig. 12. Verification with time-domain simulation.

ON-time fraction specification (e.g., 40%), a designer can reduce the required capacitance size by roughly an order of magnitude by choosing a larger V_{MAX} (e.g., 10 versus 2 V). Additionally, the analysis displays that, for a given V_{MAX} choice, there is an optimal C beyond which larger capacitance values actually yield a reduced total ON-time fraction.

For verification, a time-domain numerical simulation (in compressed time) of the harvester unit was implemented, and the results were compared with those of the Markov chain analysis. The simulation used the same parameters listed above for the Markov chain analysis. The state variable of the simulation is the storage capacitor voltage (and thus the stored energy). Exponential random variables for the arrival times of electromechanical load turn-ons and the arrival magnitudes of net accumulated energy for each arrival were implemented with the λ and E_{NET} parameters presented above. The time-domain simulation selects several realizations of these random variables. Over a total simulation length of 10 000 h in compressed time, the stored energy is calculated at fine timesteps. Clamping the stored energy between the $E_{LOW} = 0$ and E_{MAX} bounds as necessary, the simulation calculates and updates the stored energy at each time step according to the device power consumption, self-discharge, and the realization of the stochastic energy harvest variables. Fig. 12 displays the Markov chain results with a corresponding time-domain simulation. There is excellent agreement at $V_{MAX} = 8$ V, and the simulations match similarly across other voltage levels.

VI. Conclusion

This work presented a mathematical framework for sizing capacitive energy storage units of batteryless sensors. A statistical power consumption profile of an electromechanical machine was presented. From these experimental power measurements, a power harvest profile for a magnetic energy harvester was developed and used to inform two practical sensor design examples, one which emphasizes fast start-up in response to environmental events and another which emphasizes high ON-time throughout periods of no energy harvest. Our design examples underscore both the capacitance and V_{START} and V_{MAX} storage voltage thresholds as design variables that work in tandem to deliver a satisfactory storage stage for servicing a batteryless sensor. Leveraging the interplay between C and its voltage opens design opportunities for reducing capacitor size and thus overall system volume at the "cost" of higher voltage thresholds or reducing voltage thresholds at the "cost" of larger storage capacitance. Furthermore, our results indicate that excessively large storage capacitances actually contribute to reduced total fractional ON-time when considering intermittent sensor operation over long time periods. Future work aims to apply this guide to a variety of industrial equipment from which statistically informed power harvest profiles can be extracted for design. For verification, field deployment of a batteryless energy harvesting sensor with storage designed according to the above guidelines also warrants further efforts.

References

[1] Y. Chen et al., "A review of lithium-ion battery safety concerns: The issues, strategies, and testing standards," *J. Energy Chem.*, vol. 59, pp. 83–99, Aug. 2021. [Online]. Available: https://www.sciencedirect.com/science/article/pii/S2095495620307075

[2] T. Ruan, Z. J. Chew, and M. Zhu, "Energy-aware approaches for energy harvesting powered wireless sensor nodes," *IEEE Sensors J.*, vol. 17, no. 7, pp. 2165–2173, Apr. 2017.

[3] D. Monagle, E. A. Ponce, and S. B. Leeb, "Rule the joule: An energy management design guide for self-powered sensors," *IEEE Sensors J.*, vol. 24, no. 1, pp. 6–15, Jan. 2024.

[4] A. K. Sultania and J. Famaey, "Batteryless Bluetooth low energy prototype with energy-aware bidirectional communication powered by ambient light," *IEEE Sensors J.*, vol. 22, no. 7, pp. 6685–6697, Apr. 2022.

[5] D. Balsamo, O. Cetinkaya, A. R. Arreola, S. C. B. Wong, G. V. Merrett, and A. S. Weddell, "A control flow for transiently powered energy harvesting sensor systems," *IEEE Sensors J.*, vol. 20, no. 18, pp. 10687–10695, Sep. 2020.

[6] M. Zhu, M. Hassanalieragh, Z. Chen, A. Fahad, K. Shen, and T. Soyata, "Energy-aware sensing in data-intensive field systems using supercapacitor energy buffer," *IEEE Sensors J.*, vol. 18, no. 8, pp. 3372–3383, Apr. 2018.

[7] S. Jung, S. Kim, W. Cho, and K. Lee, "Development of highly efficient energy harvester based on magnetic field emanating from a household power line and its autonomous interface electronics," *IEEE Sensors J.*, vol. 23, no. 7, pp. 6607–6615, Apr. 2023.

[8] S. Chamanian, S. Baghaee, H. Uluşan, Ö. Zorlu, E. Uysal-Biyikoglu, and H. Külah, "Implementation of energy-neutral operation on vibration energy harvesting WSN," *IEEE Sensors J.*, vol. 19, no. 8, pp. 3092–3099, Apr. 15, 2019.

[9] T. Zhu, Z. Zhong, Y. Gu, T. He, and Z.-L. Zhang, "Leakage-aware energy synchronization for wireless sensor networks," in *Proc. 7th Int. Conf. Mobile Syst., Appl., Services*, New York, NY, USA, Jun. 2009, pp. 319–332, doi: 10.1145/1555816.1555849.

[10] D. Balsamo, A. S. Weddell, G. V. Merrett, B. M. Al-Hashimi, D. Brunelli, and L. Benini, "Hibernus: Sustaining computation during intermittent supply for energy-harvesting systems," *IEEE Embedded Syst. Lett.*, vol. 7, no. 1, pp. 15–18, Mar. 2015.

[11] B. Islam and S. Nirjon, "Scheduling computational and energy harvesting tasks in deadline-aware intermittent systems," in *Proc. IEEE Real-Time Embedded Technol. Appl. Symp. (RTAS)*, Jun. 2020, pp. 95–109.

[12] B. Srbinovski, M. Magno, B. O'Flynn, V. Pakrashi, and E. Popovici, "Energy aware adaptive sampling algorithm for energy harvesting wireless sensor networks," in *Proc. IEEE Sensors Appl. Symp. (SAS)*, Apr. 2015, pp. 1–6.

[13] A. Soroudi, M. Aien, and M. Ehsan, "A probabilistic modeling of photo voltaic modules and wind power generation impact on distribution networks," *IEEE Syst. J.*, vol. 6, no. 2, pp. 254–259, Jun. 2012.

[14] H.-I. Su and A. E. Gamal, "Modeling and analysis of the role of energy storage for renewable integration: Power balancing," *IEEE Trans. Power Syst.*, vol. 28, no. 4, pp. 4109–4117, Nov. 2013.

Authorized licensed use limited to: MIT. Downloaded on June 04,2026 at 16:36:13 UTC from IEEE Xplore. Restrictions apply.

[15] X. Wang, M. Yue, E. Muljadi, and W. Gao, "Probabilistic approach for power capacity specification of wind energy storage systems," *IEEE Trans. Ind. Appl.*, vol. 50, no. 2, pp. 1215–1224, Mar. 2014.

[16] Y. Zahraoui, T. Korõtko, A. Rosin, and R. Ahmadiahangar, "Stochastic energy management for battery storage system-based microgrid considering different forecasting models," in *Proc. IEEE 17th Int. Conf. Compat., Power Electron. Power Eng. (CPE-POWERENG)*, Jun. 2023, pp. 1–6.

[17] M. Manohar, E. Koley, and S. Ghosh, "Stochastic weather modeling-based protection scheme for hybrid PV–wind system with immunity against solar irradiance and wind speed," *IEEE Syst. J.*, vol. 14, no. 3, pp. 3430–3439, Sep. 2020.

[18] B. P. Mann, D. A. Barton, and B. A. Owens, "Uncertainty in performance for linear and nonlinear energy harvesting strategies," *J. Intell. Mater. Syst. Struct.*, vol. 23, no. 13, pp. 1451–1460, Sep. 2012.

[19] R. Madankan, M. A. Karami, and P. Singla, "Uncertainty analysis of energy harvesting systems," in *Proc. Int. Design Eng. Tech. Conf. Comput. Inf. Eng. Conf.*, vol. 6, Aug. 2014, pp. 1–7, doi: 10.1115/DETC2014-35480.

[20] M. Kulik, R. Gabor, and M. Jagieła, "Surrogate model for design uncertainty estimation of nonlinear electromagnetic vibration energy harvester," *Energies*, vol. 15, no. 22, p. 8601, Nov. 2022. [Online]. Available: https://www.mdpi.com/1996-1073/15/22/8601

[21] A. Cammarano, C. Petrioli, and D. Spenza, "Online energy harvesting prediction in environmentally powered wireless sensor networks," *IEEE Sensors J.*, vol. 16, no. 17, pp. 6793–6804, Sep. 2016.

[22] D. Altinel and G. K. Kurt, "Modeling of multiple energy sources for hybrid energy harvesting IoT systems," *IEEE Internet Things J.*, vol. 6, no. 6, pp. 10846–10854, Dec. 2019.

[23] L. Sigrist, R. Ahmed, A. Gomez, and L. Thiele, "Harvesting-aware optimal communication scheme for infrastructure-less sensing," *ACM Trans. Internet Things*, vol. 1, no. 4, pp. 1–26, Jun. 2020, doi: 10.1145/3395928.

[24] R. R. Rout, M. S. Krishna, and S. Gupta, "Markov decision process-based switching algorithm for sustainable rechargeable wireless sensor networks," *IEEE Sensors J.*, vol. 16, no. 8, pp. 2788–2797, Apr. 2016.

[25] J. Gao, R. Wu, J. Hao, C. Xu, and H. Guo, "SWIPT-based energy scheduling for solar-powered WSN in full-duplex mode," *IEEE Sensors J.*, vol. 22, no. 13, pp. 13668–13681, Jun. 2022.

[26] R. Ahmed, S. Draskovic, and L. Thiele, "Stochastic guarantees for adaptive energy harvesting systems," *IEEE Trans. Comput.-Aided Design Integr. Circuits Syst.*, vol. 41, no. 11, pp. 3614–3625, Nov. 2022.

[27] B. Munir and V. Dyo, "On the impact of mobility on battery-less RF energy harvesting system performance," *Sensors*, vol. 18, no. 11, p. 3597, Oct. 2018. [Online]. Available: https://www.mdpi.com/1424-8220/18/11/3597

[28] D. Fan, L. L. Ruiz, J. Gong, and J. Lach, "EHDC: An energy harvesting modeling and profiling platform for body sensor networks," *IEEE J. Biomed. Health Informat.*, vol. 22, no. 1, pp. 33–39, Jan. 2018.

[29] Z. Yuan, Y. Ge, J. Wei, S. Yuan, R. Liu, and X. Mo, "Energy prediction for energy-harvesting wireless sensor: A systematic mapping study," *Electronics*, vol. 12, no. 20, p. 4304, Oct. 2023. [Online]. Available: https://www.mdpi.com/2079-9292/12/20/4304

[30] Joulescope. *Joulescope JS220: Precis. Energy Analyzer*. Accessed: Apr. 2025. [Online]. Available: https://www.joulescope.com/products/js220-joulescope-precision-energy-analyzer

[31] P. Dutta, M. Feldmeier, J. Paradiso, and D. Culler, "Energy metering for free: Augmenting switching regulators for real-time monitoring," in *Proc. Int. Conf. Inf. Process. Sensor Netw.*, Apr. 2008, pp. 283–294.

[32] J. Brusey, J. Kemp, E. Gaura, R. Wilkins, and M. Allen, "Energy profiling in practical sensor networks: Identifying hidden consumers," *IEEE Sensors J.*, vol. 16, no. 15, pp. 6072–6080, Aug. 2016.

[33] B. Martinez, M. Montón, I. Vilajosana, and J. D. Prades, "The power of models: Modeling power consumption for IoT devices," *IEEE Sensors J.*, vol. 15, no. 10, pp. 5777–5789, Oct. 2015.

[34] A. Sabo and S. M. Qaisar, "The event-driven power efficient wireless sensor nodes for monitoring of insects and health of plants," in *Proc. IEEE 3rd Int. Conf. Signal Image Process. (ICSIP)*, Jul. 2018, pp. 478–483.

[35] M. Rusci, D. Rossi, M. Lecca, M. Gottardi, E. Farella, and L. Benini, "An event-driven ultra-low-power smart visual sensor," *IEEE Sensors J.*, vol. 16, no. 13, pp. 5344–5353, Jul. 2016.

[36] J. Moon and S. B. Leeb, "Wire less sensors for electromechanical systems diagnostics," *IEEE Trans. Instrum. Meas.*, vol. 67, no. 9, pp. 2235–2246, Sep. 2018.

[37] R. Zachar, P. Lindahl, J. Donnal, W. Cotta, C. Schantz, and S. B. Leeb, "Utilizing spin-down transients for vibration-based diagnostics (Don't short) of resiliently mounted machines," *IEEE Trans. Instrum. Meas.*, vol. 65, no. 7, pp. 1641–1650, Jul. 2016.

[38] J. Paris, J. S. Donnal, R. Cox, and S. Leeb, "Hunting cyclic energy wasters," *IEEE Trans. Smart Grid*, vol. 5, no. 6, pp. 2777–2786, Nov. 2014.

[39] R. G. Gallager, *Discrete Stochastic Processes*. New York, NY, USA: Springer, 1996.

[40] D. Monagle, E. Ponce, and S. B. Leeb, "Resonant circuits for split-core magnetic energy harvesters," *IEEE Trans. Ind. Electron.*, vol. 71, no. 8, pp. 9932–9941, Aug. 2024.

[41] K. Corporation. (2020). *Supercapacitor Leakage Self Discharge Characteristics*. [Online]. Available: https://www.kemet.com/en/us/technical-resources/supercapacitor-leakage-self-discharge-characteristics.html

Daniel Monagle (Graduate Student Member, IEEE) received the B.S. and M.S. degrees in electrical engineering and computer science from Massachusetts Institute of Technology, Cambridge, MA, USA, in 2020 and 2022, respectively, where he is currently pursuing the Ph.D. degree.

His research interests include energy harvesting, magnetics, low-power circuit design, and self-powered systems.

Mr. Monagle was awarded the MIT School of Engineering from 2023 to 2024 Thomas G. Stockham Jr. Fellowship for excellence in teaching and mentoring.

Thomas C. Krause (Graduate Student Member, IEEE) received the B.S. degree in electrical engineering from Purdue University, West Lafayette, IN, USA, in 2019, and the M.S. and E.E. degrees in electrical engineering and computer science from Massachusetts Institute of Technology, Cambridge, MA, USA, in 2021 and 2024, respectively, where he is currently pursuing the Ph.D. degree.

Aaron W. Langham (Graduate Student Member, IEEE) received the B.E.E. degree in electrical engineering from Auburn University, Auburn, AL, USA, in 2018, and the M.S. and E.E. degrees in electrical engineering and computer science from Massachusetts Institute of Technology, Cambridge, MA, USA in 2022 and 2024, respectively, where he is currently pursuing the Ph.D. degree.

His research interests include signal processing, machine learning, and IoT platforms for energy systems.

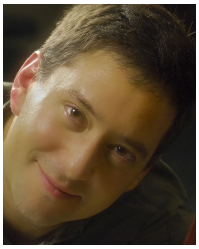

Steven B. Leeb (Fellow, IEEE) received the Ph.D. degree from Massachusetts Institute of Technology (MIT), Cambridge, MA, USA, in 1993.

He has served as a Commissioned Officer for the USAF reserves. Since 1993, he has been a Faculty Member with the Department of Electrical Engineering and Computer Science, MIT. He also holds a joint appointment with the Department of Mechanical Engineering, MIT. He is the author or co-author of over 200 publications and 20 U.S. patents in the fields of electromechanics and power electronics.

Authorized licensed use limited to: MIT. Downloaded on June 04,2026 at 16:36:13 UTC from IEEE Xplore. Restrictions apply.